Quantum chaos of a particle in a square well: Competing length scales and dynamical localization

R. Sankaranarayanan,* A. Lakshminarayan,† and V. B. Sheorey‡
Physical Research Laboratory, Navrangpura, Ahmedabad 380 009, India
(Received 5 May 2001; published 21 September 2001)

The classical and quantum dynamics of a particle trapped in a one-dimensional infinite square well with a time-periodic pulsed field is investigated. This is a two-parameter non-KAM (Kolmogorov-Arnold-Moser) generalization of the kicked rotor, which can be seen as the standard map of particles subjected to both smooth and hard potentials. The virtue of the generalization lies in the introduction of an extra parameter R, which is the ratio of two length scales, namely, the well width and the field wavelength. If R is a noninteger the dynamics is discontinuous and non-KAM. We have explored the role of R in controlling the localization properties of the eigenstates. In particular, the connection between classical diffusion and localization is found to generalize reasonably well. In unbounded chaotic systems such as these, while the nearest neighbor spacing distribution of the eigenvalues is less sensitive to the nature of the classical dynamics, the distribution of participation ratios of the eigenstates proves to be a sensitive measure; in the chaotic regimes the latter is log-normal. We find that the tails of the well converged localized states are exponentially localized despite the discontinuous dynamics while the bulk part shows fluctuations that tend to be closer to random matrix theory predictions. Time evolving states show considerable R dependence, and tuning R to enhance classical diffusion can lead to significantly larger quantum diffusion for the same field strengths, an effect that is potentially observable in present day experiments.

DOI: 10.1103/PhysRevE.64.046210 PACS number(s): 05.45.Mt, 72.15.Rn, 68.65.Fg

I. INTRODUCTION

For several years now studies on quantized chaotic systems have increased significantly with the object of revealing quantum mechanical manifestations of classical chaos [1,2]. The bulk of the work has used smooth Hamiltonian systems. If we start perturbing an integrable system, classical Hamiltonian chaos may develop through a gradual destruction of invariants. The celebrated Kolmogorov-Arnold-Moser (KAM) theorem gives conditions as to when a given torus will be only distorted. This scenario has been widely studied in two-degree-of-freedom systems or two-dimensional area preserving maps. However, there are conditions upon which the KAM theorem rests that may not always be satisfied by certain systems of physical interest. In particular, if the perturbation is not sufficiently smooth or even discontinuous the KAM scenario may break down. Large scale chaos may instantaneously develop in the system. One other way that the KAM scenario fails is when the unperturbed system is fully resonant, as in the Kepler problem. We deal in this paper with the former kind of non-KAM behavior.

We first discuss the prevalence of systems where such effects may be seen. The simplest systems where Hamiltonian chaos can develop are the so called 1.5-degree-of-freedom system, which are time-dependent one-degree-of-freedom systems. Thus we consider the rotor Hamiltonian

$$H=\frac{p_\theta^2}{2}+f(t)V(\theta),$$

where $V(\theta)$ is an external potential that is periodic with period 2π, and $f(t)$ is a periodic function of time with period T. A lengthening pendulum, for instance, may be the system under study. If $V(\theta)$ is sufficiently smooth, the KAM theorem scenario combined with the Poincaré-Birkhoff theorem provides the generic behavior. The smoothness or at least continuity of $V(\theta)$ is provided by the periodic boundary conditions in the angular position of the rotor. Introducing discontinuous potentials will lead to δ function forces equivalent to walls of certain heights.

This brings us to a natural class of systems where non-KAM behavior will be the rule rather than the exception: externally forced particles in wells. This forms a broad class of systems that have evoked considerable interest and research since the development of quantum wells and dots. One of the experiments where quantum ''scarring'' of wave functions was reported involved resonant tunneling of a particle across a well in which there were external electromagnetic fields [3].

In fact the simplest of such systems involve a particle in one-dimensional infinite square wells (1D billiards) with time-dependent external fields. Consider as an example the Hamiltonian

$$H=H_0+\epsilon\cos(\omega t)\cos(2\pi x/\lambda), \tag{1}$$

where $H_0=p^2/2+V_{sq}(x;a)$, describing such a particle. The potential $V_{sq}(x;a)$ is the confining infinite square well potential of width $2a$, centered at the origin. Here ϵ and λ are the field strength and wavelength of the external field which is being modulated in time with frequency ω.

It is easy to verify that the equations of motion are invariant under the following transformation:

$$t\to\omega_0 t,\quad p\to p/2a\omega_0,\quad x\to x/2a,$$

*Electronic address: sankar@prl.ernet.in
†Electronic address: arul@prl.ernet.in
‡Electronic address: sheorey@prl.ernet.in

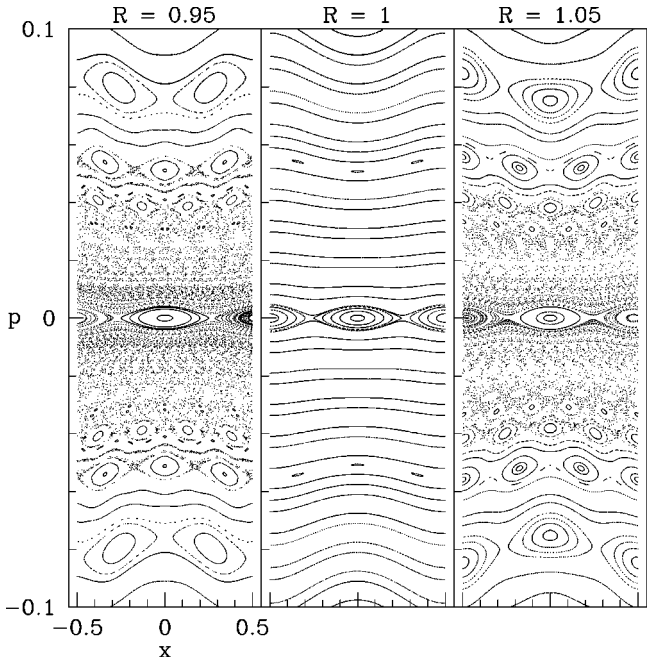

FIG. 1. Typical phase space of the system governed by the Hamiltonian (1) with $\epsilon=0.001$ and $\omega=1$. The lower momentum region is increasingly chaotic when the length scales do not match.

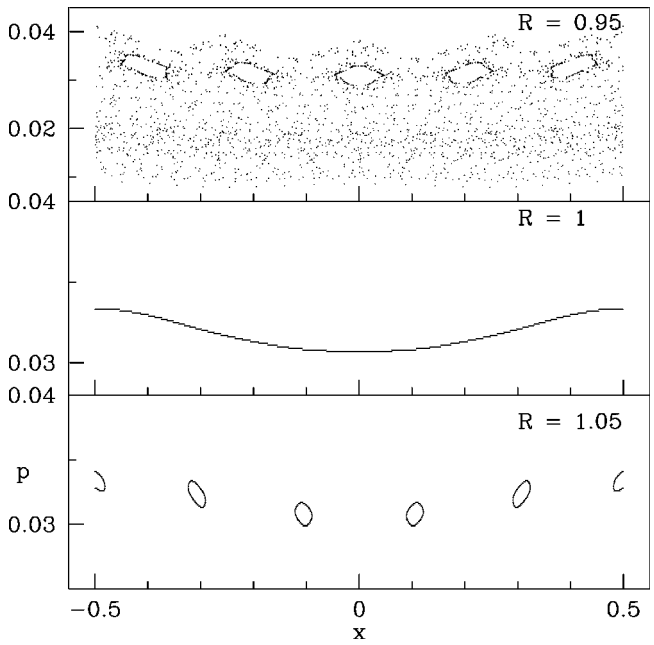

FIG. 2. Shown are orbits of Fig. 1 having identical initial conditions. The initial condition corresponds to a KAM torus in the lower momentum region for $R=1$ (the negative momentum region is not shown here). Note the abrupt change in stability and the nongeneric features of the resultant phase space structures.

and

$$\epsilon\rightarrow\epsilon/(2a\omega_0)^2, \quad \lambda\rightarrow\lambda/2a, \quad \omega\rightarrow\omega/\omega_0.$$

Here the frequency ω_0, which sets the new time scale, is arbitrary. Note that the new scaled variables and parameters are referred to by the old symbols and they are dimensionless. Setting $\omega_0=\omega$ in the above transformation, we have effectively two parameters: ϵ and $R=2a/\lambda$. Here R is the ratio of the two length scales of the system, i.e., the well width and field wavelength. The presence of two competing length scales provides a rich range of non-KAM behaviors. In particular, if the dimensionless ratio R is a noninteger there is the possibility of observing non-KAM phenomena.

Under the perturbation we can expect roughly that states whose absolute value of the initial momentum is less than $\sqrt{2|\epsilon|}$ will be most affected. Thus low energy states will be most affected by the time-dependent forces. Figure 1 shows the effect of the parameter R. While for $R=1$ the system is essentially KAM and has KAM tori interspersed with resonances, any small deviation of R away from unity destroys low energy KAM curves and leads to increased chaos. Figure 2 shows the fate of an individual KAM torus for which $R=1$ is a ''bifurcation'' point in parameter space and which changes stability on either side. We expect such behavior to be generic to a large class of similar systems and in this paper we will exhaustively study a ''standard map'' version of these systems. Just as the standard map provides an abstract view of behavior around nonlinear resonances, we expect our model's analysis to provide such a view for these systems.

Many models have been studied where the time dependence $f(t)$ is a train of Dirac δ functions, the periodically kicked systems [4]. The reasons are evident: they are the simplest Hamiltonian systems where many generic features of chaotic complex systems may be observed; and they allow a partial integration of the equations of motion, from kick-to-kick, enabling us to study iterative ''mappings'' rather than differential equations. Quantum mechanically the simplification enables us to partially integrate the Schrödinger equation and write the kick-to-kick propagator, or Floquet operator, analytically [5].

An important paradigm in this class is the δ kicked rotor from which is derived the standard map [6,7]. The dynamical richness of the classical system that obeys the KAM theorem and the consequent smooth transition to chaos are now well known and fairly well understood [8–10]. The corresponding quantum system has also been studied quite extensively as a model of ''quantum chaos'' (see [11] for an early review of this), and continues to provide an excellent model to numerically test our understanding of such systems [12].

The periodic input of energy into the system through the kicks can result in a diffusive increase of the momentum, and strong kicking strength can lead to unbounded energy growth classically. However, an important result of quantization is that the eigenfunctions (quasienergy states) are generically *exponentially localized in momentum space*, which suppresses the momentum diffusion even in the highly chaotic regime. A plausible mechanism for this ''dynamical localization'' was suggested when an analogy was found [13] to Anderson type localization of electrons in random on-site potentials [14]. Experimental realizations of the δ kicked rotor, with cold atoms in pulsed standing laser fields [15], have confirmed the quantum suppression of diffusion. The localized states in unbounded momentum space result in quasi-

independence of the quasienergies, and the random matrix properties [16,1] expected of quantized chaotic systems are not seen. For instance, the nearest neighbor spacing distribution is Poisson rather than Wigner and the eigenfunction components are not Gaussian distributed. It must be stated that most of these results are numerical and larger matrix calculations that are ''more semiclassical'' may show spectral transitions as the bulk of the eigenfunctions spread out and overlap with each other while the tails are still exponentially localized. Some evidence of this will also be presented in this paper.

Following our motivational discussion above, we replace the time dependence by a series of δ functions to facilitate the derivation of a map in which we can study non-KAM behavior of the kind suggested above. Recently study of such systems has begun [17,18]. For instance, in [17] it is shown that the quantum states are extended and delocalized in the highly chaotic (strong field) regime. In turn, the spacing of the quasienergies, unlike in the kicked rotor, follows the Wigner distribution. It is argued that the extended states do overlap and hence the corresponding quasienergies are not independent, resulting in level repulsion. Part of the present paper also critically examines these results. In [18] a classical analysis of a generalized system was carried out to understand the changes of stability that occur as a function of R and some of these results will be summarized below.

II. CLASSICAL SYSTEM

The system of interest is a particle inside the potential $V_{sq}(x;a)$ in the presence of a particular time-periodic impulse. We consider the Hamiltonian given by

$$H=H_0+\epsilon\cos(2\pi x/\lambda)\sum_{n=-\infty}^{\infty}\delta(n-t/T). \tag{2}$$

The kick-to-kick dynamics of the particle immediately after each pulse can be described by an area preserving map which in dimensionless form is

$$\begin{aligned} X_{n+1}&=(-1)^{B_n}\{(X_n+P_n)-\mathrm{sgn}(P_n)B_n\},\\ P_{n+1}&=(-1)^{B_n}P_n+(K/2\pi)\sin(2\pi RX_{n+1}). \end{aligned} \tag{3}$$

Here $B_n=[\mathrm{sgn}(P_n)(X_n+P_n)+1/2]$ is the number of bounces of the particle between the walls during the interval between the nth and $(n+1)$th kick, and $[\cdots]$ stands for the integer part of the argument. The state of the particle just after the nth kick is now given in the new variables as X_n, P_n. The sign of the momentum (± 1) is given by $\mathrm{sgn}(P_n)$. The following scaling relations are used to redefine the variables and parameters:

$$X_n=\frac{x_n}{2a},\quad P_n=\frac{p_nT}{2a},\quad K=\frac{2\epsilon\pi^2T^2}{a\lambda},\quad R=\frac{2a}{\lambda}. \tag{4}$$

We note that $|X_n|\leqslant 1/2$ and effective parameters of the particle dynamics are K, the field strength, and R, the ratio of the two length scales. The map in (3) shows the principal features that we discussed earlier in the Introduction and may qualify as a ''standard'' map for such non-KAM systems. In fact there is a close relationship between this ''well map'' (3) and the standard map itself that allows us to study it as a *generalized standard map* (GSM) [18]. This is the map

$$\begin{aligned} P_{n+1}&=P_n+(K/2\pi)\sin(2\pi RX_n),\\ X_{n+1}&=X_n+P_{n+1}\pmod 1, \end{aligned} \tag{5}$$

which is defined on a cylinder $(-\infty,\infty)\times[-1/2,1/2)$. The well map and the GSM differ only in boundary conditions, i.e., the former and latter have reflective and periodic boundary conditions, respectively. It is easy to see that this does not play any effective role, in the sense that the trajectories as evolved under the two systems can at most differ by a sign, depending on the number of bounces undergone. This fact considerably simplifies our analysis of the well map. When $R=1$, the GSM is the well studied and fairly well understood standard map of the δ-kicked rotor.

The dynamics of the GSM is highly chaotic and diffusive in the strong field regime $(K\gg 1)$. In addition, it exhibits other interesting features like the development of chaos and hence diffusion even in the weak field regime $(K<1)$ when $R\neq j$ where j is a positive integer (see Fig. 3). Note that the phase space portraits of both the well map and the GSM are same. Such dynamical features are in fact common in non-KAM systems, and one such situation is shown earlier. We can understand the development of chaos at low field strengths from the observation that the otherwise continuous map is discontinuous when $R\neq j$. The KAM theorem does not hold for the discontinuous case and no smooth KAM tori

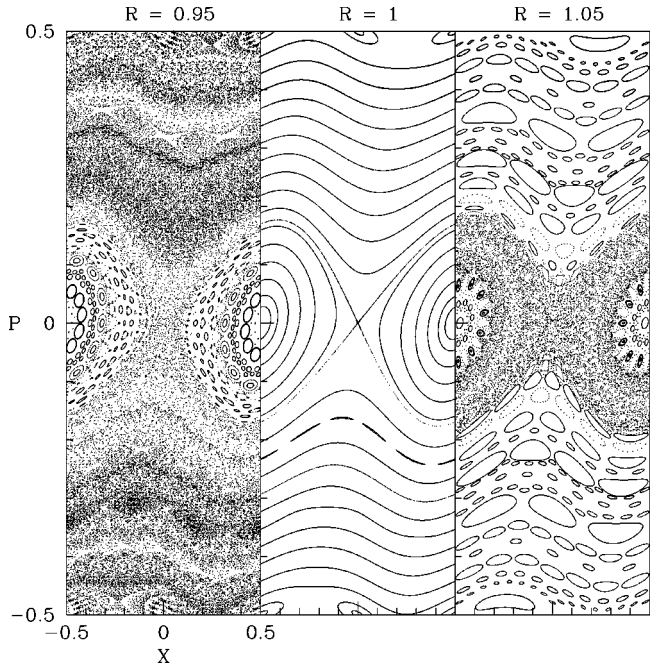

FIG. 3. Phase space portrait of the GSM with $K=0.3$. For $R=1$, the dynamics is nearly regular wherein many smooth KAM tori are seen. When R departs from unity the dynamics is increasingly complex and no KAM tori are seen. This may be compared to the lower momentum region in Fig. 1.

exist in the phase space, however small K may be. In the absence of KAM tori, the phase space is chaotic and diffusive even in the weak field regime. Moreover, when $R<1/2$ the GSM is a hyperbolic system. For a more detailed investigation of the GSM we refer the reader to [18].

III. QUANTUM MECHANICS OF THE TRAPPED PARTICLE

For a Hamiltonian that is periodic in time with period T $(=2\pi/\omega)$, solutions of the Schrödinger equation satisfy the eigenvalue equation [19]

$$U|\psi_j\rangle = e^{-i\alpha_j T/\hbar}|\psi_j\rangle, \tag{6}$$

where U is the one-period time evolution operator. Here $|\psi_j\rangle$ and α_j are the quasienergy, states and quasienergies, respectively. It is to be noted that the inner product of two arbitrary solutions of the Schrödinger equation for an arbitrary time-dependent Hamiltonian is independent of time due to the Hermiticity of the Hamiltonian. As a consequence of this, states corresponding to α_i and α_j such that $\alpha_i-\alpha_j\neq n\hbar\omega$ (where n is an integer) are orthogonal at a given time. If $\alpha_i-\alpha_j=n\hbar\omega$, the states are degenerate and hence the quasienergies are uniquely defined modulo $\hbar\omega$. From the set of all orthogonal states we may write the general solution at a given time as $|\Psi\rangle=\Sigma_j c_j|\psi_j\rangle$.

A. Matrix representation of U

Periodically kicked systems are particularly easy to study since U can be written immediately by integrating the Schrödinger equation between successive kicks. For the Hamiltonian H in Eq. (2) we have

$$U=\exp\left\{-ik\cos\left(\frac{2\pi x}{\lambda}\right)\right\}\exp\left\{-i\frac{H_0 T}{\hbar}\right\}, \tag{7}$$

where $k=\epsilon T/\hbar$. Note that the above time evolution operator is the quantum counterpart of the well map and not that of the GSM. The eigensystem in Eq. (6) may be solved by diagonalizing a matrix representation of U. The natural choice of basis for the U matrix is the eigenstates of the unperturbed Hamiltonian H_0:

$$H_0|n\rangle=E_n|n\rangle, \tag{8}$$

where $n=1,2,3,\ldots$. The energy eigenfunctions and eigenvalues are

$$\langle x|n\rangle=\begin{cases}\dfrac{1}{\sqrt{a}}\cos\left(\dfrac{n\pi x}{2a}\right) & \text{for } n \text{ odd},\\[2ex] \dfrac{1}{\sqrt{a}}\sin\left(\dfrac{n\pi x}{2a}\right) & \text{for } n \text{ even},\end{cases} \qquad E_n=\frac{n^2\pi^2\hbar^2}{8a^2}. \tag{9}$$

The unitary matrix U is then calculated as

$$\begin{aligned}U_{mn}&=\langle m|U|n\rangle\\ &=\langle m|\exp\{-ik\cos(2\pi x/\lambda)\}|n\rangle e^{-in^2\tau}\equiv F_{mn}e^{-in^2\tau},\end{aligned} \tag{10}$$

where we have defined an effective Planck constant as

$$\tau=\frac{\pi^2\hbar T}{8a^2}. \tag{11}$$

As the external field preserves parity we have

$$F_{mn}=\begin{cases}0 & \text{if } m+n \text{ is odd}\\ \dfrac{1}{2\pi}\{Q_{(m-n)/2}-(-1)^n Q_{(m+n)/2}\} & \text{if } m+n \text{ is even},\end{cases} \tag{12}$$

where

$$Q_l=\int_{-\pi}^{\pi}\cos(l\theta)e^{-ik\cos(R\theta)}d\theta \tag{13}$$

and $\theta=\pi x/a$. We note that Q_l is a Bessel function integral for integer R, while for noninteger R the integral constitutes a kind of ''incomplete'' Bessel function. Invoking the Bessel function $J_s(k)$ through the identity

$$e^{-ik\cos\theta}=\sum_{s=-\infty}^{\infty}(-i)^s J_s(k)e^{-is\theta}$$

the integral can be evaluated as a series:

$$Q_l=2\pi J_0(k)\delta_{l,0}+2\sum_{s=1}^{\infty}(-i)^s J_s(k)C_s, \tag{14}$$

where

$$\begin{aligned}C_s&=\int_{-\pi}^{\pi}\cos(l\theta)\cos(sR\theta)d\theta\\ &=\begin{cases}\dfrac{(-1)^l 2sR\sin(sR\pi)}{(sR)^2-l^2} & \text{for } sR\neq|l|\\ \pi & \text{for } sR=|l|.\end{cases}\end{aligned}$$

The relation $J_{-s}(k)=(-1)^s J_s(k)$ has been used in Eq. (14). Note that if R is an integer Eq. (14) simplifies to

$$Q_l=2\pi\sum_{s=0}^{\infty}(-i)^s J_s(k)\delta_{|l|,sR} \tag{15}$$

and a single term is picked out of the infinite series.

The forms of Q_l allow us to assess the fall of the matrix elements of the unitary matrix U. For integer R the unitary matrix can be essentially banded as the matrix elements fall off exponentially after a certain cutoff. For $R=1$, as is well known and can be seen from above for $l>k$ the matrix elements fall off exponentially, where l measures the distance from the diagonal. On the other hand when R is not an inte-

ger, apart from the Bessel function terms there are terms that are decreasing only polynomially in l. For instance, when $R=1/2$ we have

$$Q_l = 2\pi(-1)^l J_{2l}(k) + (-1)^l 8 \times \sum_{s=1,3,5,\ldots}^{\infty} \frac{(-i)^s s \sin(s\pi/2)}{s^2-4l^2} J_s(k). \quad (16)$$

The infinite series gets effectively cut off for $s>k$. The finite sum has terms that only decay as l^{-2}. Thus noninteger R values imply an important characteristic of the unitary quantum map: the polynomial fall of matrix elements, as opposed to the exponential fall characterizing integer R. In fact, we may speculate whether non-KAM systems are *always* characterized by polynomially decaying matrix elements in the unperturbed basis. According to earlier studies eigenfunction localization crucially depends on the way in which matrix elements decrease.

When $R=1$, the classical equivalence of the kicked rotor to the particle in a well was noted above. It is easy to see that the equivalence persists quantum mechanically also. The parity symmetry reduced rotor unitary matrix is identical to the well unitary operator in this case and hence odd states of the rotor correspond to odd states of the well, while the even states have a similar relationship. Thus all that is known for the quantum standard map, including exponential localization of eigenstates, may be carried over to the well system with $R=1$. This allows us to address interesting questions of deviations from the standard map in a single model.

The perturbing potential $\cos(2\pi x/\lambda)$ preserves the parity of H_0, and hence U has symmetry of parity. In what follows we consider only the states that have odd parity. In addition, the system has spatial translational symmetry when R is an integer. Let us define a transformation for integer R as

$$\mathcal{T}f(X) = f((X+1/R) \mod 1) \quad (17)$$

such that $\mathcal{T}^R f(X) = f(X)$. $\mathcal{T}$ has the eigenvalues $\beta_l = \exp(i2l\pi/R)$, where $l=0,1,2,\ldots,(R-1)$. The commutation relation $[U,\mathcal{T}]=0$ leading to $\mathcal{T}|\psi\rangle = \beta_l|\psi\rangle$. For $R=2$, $\beta_l=\pm 1$; in this case we consider only the states that correspond to $\beta_l=1$.

The dimensionless quantum parameters k and τ are related to the classical parameters through the relation $K/R = 8k\tau$. The semiclassical limit is $k\to\infty$ and $\tau\to 0$, such that $k\tau$ is fixed. Any arbitrary state of the system at a given time is $|\Psi(t)\rangle = \Sigma_n A_n(t)|n\rangle$ and its time evolution is given by $A_m(t+T) = \Sigma_n U_{mn} A_n(t)$.

B. Quantum resonance

Here we investigate if the parameter R has any effect on the important phenomenon of ''quantum resonance.'' We notice that the unperturbed motion of the particle, given by the Hamiltonian H_0, between the kicks simply adds phase to the wave function components [when expressed in the unperturbed basis, as in Eq. (10)]. At resonance ($\tau=2\pi$), the unperturbed motion between the kicks is absent. In this case, without loss of generality, the time evolution of an arbitrary state of the system is

$$|\Psi(t)\rangle = e^{-ik\cos(2\pi x/\lambda)t}|\Psi(0)\rangle \quad (18)$$

and thus $|\Psi(t)|^2 = |\Psi(0)|^2$. Note that here t is the number of kicks. The kinetic energy of the particle is then

$$E(t) = E(0) + \frac{-\hbar^2}{2}\left\{\left(\frac{4\pi kt}{\lambda}\right)\int_{-a}^{a}\sin\left(\frac{2\pi x}{\lambda}\right) \times \mathrm{Re}\left(i\Psi^*(0)\frac{\partial\Psi(0)}{\partial x}\right)dx - \left(\frac{2\pi kt}{\lambda}\right)^2\int_{-a}^{a}|\Psi(0)|^2\sin^2\left(\frac{2\pi x}{\lambda}\right)dx\right\}. \quad (19)$$

In the limit $t\to\infty$ the energy grows quadratically with the number of kicks. If $|\Psi(0)\rangle = |n\rangle$, i.e., the initial states is one of the unperturbed states itself, the energy is purely quadratic. In fact, the energy can be found exactly as

$$E(t) = E(0)\left\{1+\left(\frac{ktR}{n}\right)^2(2-A)\right\}, \quad (20)$$

where

$$A = \begin{cases} \dfrac{\sin(2\pi R)}{\pi R}\left(\dfrac{n^2}{n^2-4R^2}\right) & \text{if } n\neq 2R \\ (-1)^{n+1} & \text{if } n=2R. \end{cases}$$

Since $A\neq 2$, we observe that the quadratic energy growth is unaffected by the length scale ratio R. Numerically we have found that this behavior is also seen when τ is a rational multiple of 2π. Thus the quantum resonance phenomena of the well system is very similar to that of the kicked rotor [6,20]. It is to be noted that resonance is a nongeneric pure quantum phenomenon and no correspondence to it can be seen in the classical system. In the context of a particle in a well, quantum resonance may lead to enhanced ionization in a finite well.

IV. RESULTS

Having given a sufficient description of the system under investigation, here we analyze the quasienergy states and quasienergies of the generic quantum system (τ is an irrational multiple of 2π) in the relevant classical regimes. On taking a truncated N-dimensional Hilbert space spanned by the first N unperturbed basis states that belong to odd parity, diagonalization of the matrix U_{mn} gives the eigenstates $\{|\psi\rangle\}$ such that $|\psi\rangle = \Sigma_n \psi_n|n\rangle$. We consider only states that are ''converged'' in the sense that they are independent of the truncation size N. Thus the states we are interested in belong to the infinite Hilbert space; they are states of the infinite cylinder and *not* of a truncated cylinder, or torus. The last distinction becomes important as quantum states that belong to the cylinder can have completely different localization features from those that belong to a truncated cylinder. As

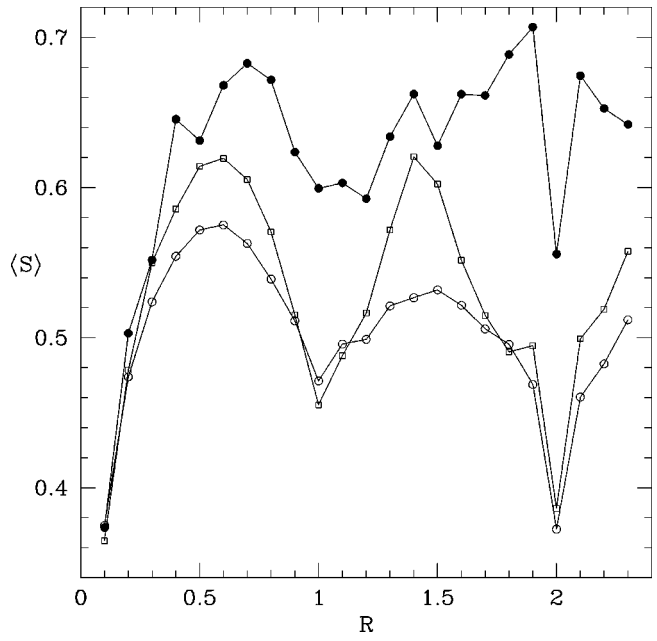

FIG. 4. Average entropy of 1000 eigenstates for $K=0.1$, $\tau=0.001$ (○); $K=1$, $\tau=0.01$ (□); $K=10$, $\tau=0.1$ (●). $N=1200$ in all cases.

we are interested in a particle in an infinite potential well, such a truncation lacks physical meaning.

A. Localization measures of eigenstates

Localization can be measured using a unified quantity, the Renyi participation ratio ξ_q,

$$\xi_q=\left(\sum_n |\psi_n|^{2q}\right)^{1/(q-1)}, \tag{21}$$

of which the entropy and participation ratio (PR) are special cases. In our analysis we first use a normalized information entropy as a measure of the localization of states, and this is defined as

$$S=\frac{-1}{\ln(N/2)}\sum_{n=1}^{N}|\psi_n|^2\ln|\psi_n|^2. \tag{22}$$

It is easy to see that $S=\ln\xi_1/\ln(N/2)$. This measure compares the entropy to that of the eigenfunctions of $N\times N$ matrices belonging to the Gaussian orthogonal ensemble (GOE) which is approximately $\ln(N/2)$. The GOE is relevant to time reversal symmetric systems such as we are considering.

First we calculate a gross measure of localization in a given spectrum by averaging over all converged states. We set criteria for the states to be converged so that the states belong to the cylinder, or are at least very close to states that belong to the cylinder. In all the following cases, the eigenvalues are converged in modulus to unity to within 0.0001 or better. Figure 4 shows the average entropy as a function of R. For small K ($\leqslant 1$), the oscillations are qualitatively similar with distinct entropy minima at integer R and maxima at around half-integer R. This may provide a simple mechanism for experimental control of the extent of localization. The information entropy is, of course, basis dependent; the unperturbed basis we use is a useful one as it has information about localization in the momentum.

Naturally, the minima in entropy are expected to have strong associations with the presence of stable regions in the classical phase space. Of special significance are KAM tori in phase space, as these structures are complete barriers to classical diffusion in momentum. In spite of the fact that in the classical system all the KAM tori break up in the standard map ($R=1$) at $K=1$, we observe a minimum entropy. This is due to the presence of cantori which are partial barriers for chaotic orbits and suppress global diffusion. For noninteger R a complex phase space picture emerges, and has been discussed in [18]. Maximum entropy around half-integer R is the classical parametric regime where the discontinuity is maximum, corresponding to maximum chaos assisted diffusion.

For large K ($=10$), oscillations in entropy are still present while there is apparently complete chaos for all relevant R values. We can understand these oscillations as due to the strong correlation between the localization of eigenstates and classical diffusion coefficient. For $R<1/2$ the semiclassical parameter $k=K/(8R\tau)$ is large, yet there is increased localization of states due to limited classical diffusion, presumably due to the presence of cantori. For the kicked rotor the exponential localization length was found to be proportional to the classical diffusion coefficient [21]. This was found by numerical experiments and is supported by certain qualitative arguments. We are now in a position to examine the relationship between quantum localization and classical diffusion in the context of the particle in a well, wherein we have the freedom of another control parameter, namely, R, with which to vary the classical diffusion.

Instead of studying localization lengths we study here measures of localization such as the entropy or the PR. We study the PR more closely than the entropy. In chaotic regimes we have numerically ascertained that the exponential of the entropy is proportional to the PR, as shown in Fig. 5. The relationship between the localization length hitherto calculated for the kicked rotor and the PR calculations we present will need more detailed study, but we expect them to be roughly proportional to each other. In fact, if we assume a fully exponentially localized state with $|\psi_n|\sim\exp(-|n-n_0|/l_\infty)$, then the PR is

$$\xi_2^{-1}=\left(\sum_n |\psi_n|^4\right)^{-1}=2l_\infty. \tag{23}$$

We recapitulate the argument connecting classical diffusion and the localization length for the specific system we are considering, as there are differences in factors. Considering the time evolution of an initial state, kinetic energy diffuses for a certain time t_c and then attains quasiperiodic saturation. The number n_c of unperturbed states that are excited during the time evolution is related to the critical time by the diffusion equation

$$\pi^2\hbar^2n_c^2=D_{\rm cl}t_c, \quad \langle(p_t-p_0)^2\rangle=D_{\rm cl}t, \tag{24}$$

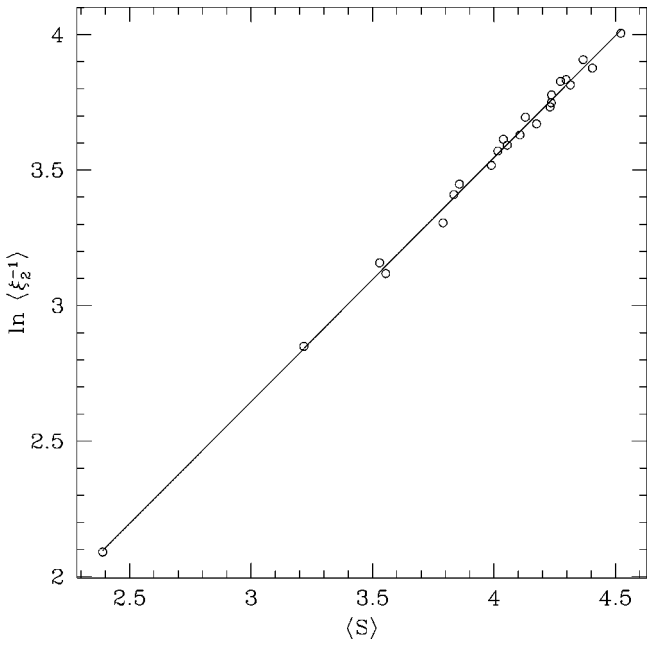

FIG. 5. Average entropy vs the logarithm of the average PR corresponding to the case $K=10$, $\tau=0.1$ of Fig. 4. The slope of the fitted straight line is 0.9 ± 0.01.

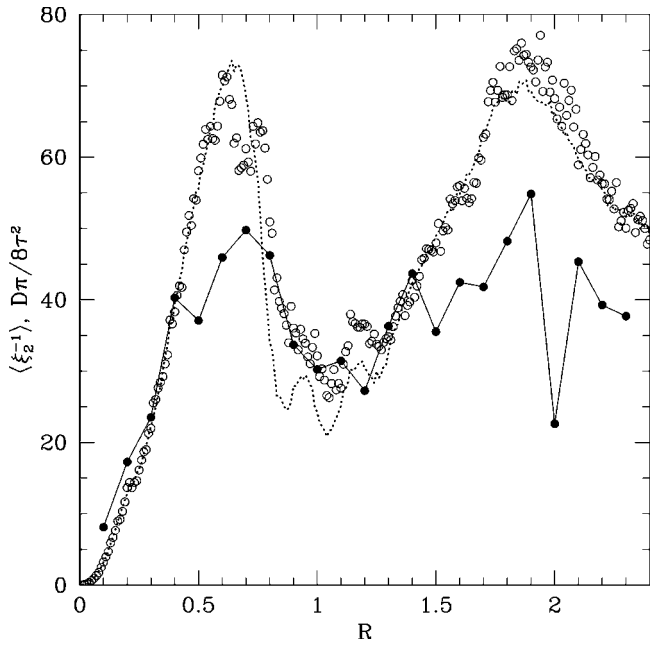

FIG. 6. The average PR (●) and the scaled classical diffusion coefficient (○) are plotted as functions of R for the case $K=10$, $\tau=0.1$. The dotted line is the scaled coefficient calculated using up to the second order time correlation. Higher order time correlations are insignificant since the classical system is highly chaotic.

where D_{cl} is the classical diffusion coefficient in momentum and $\langle\cdots\rangle$ represents the ensemble average. Here the momenta and the diffusion coefficient have dimensions and we have taken $a=1/2$. Since the critical time is the Heisenberg time relevant for n_c equally spaced eigenstates, we get $t_c \sim n_c T/2\pi$. If the average localization length $\langle l_\infty\rangle$ is also n_c, we obtain the relation

$$\langle \xi_2^{-1}\rangle = 2\langle l_\infty\rangle = \frac{\alpha\pi}{4\tau^2} D(K,R), \tag{25}$$

where τ is the dimensionless effective Planck constant defined in Eq. (11) and α is a constant whose value has been numerically determined as 1/2 for the standard map [22]. $D(K,R)$ is the dimensionless diffusion coefficient that one will get from using the dimensionless maps Eq. (3) or Eq. (5). The dependence on *both* K and R is emphasized.

In Fig. 6 we show the average PR and the scaled diffusion coefficient according to the relation Eq. (25). We see that the relation derived above holds in some parameter regions while it picks up only qualitative features of the oscillations in others. In particular, the relation seems to hold for $R<1/2$ when the classical system is hyperbolic as well as around $R=1$. The deviations from the relation (25) might be due to fluctuations of the state components in the unperturbed basis (one such case is shown in Fig. 11 below). These fluctuations may lead to different scaling behavior between the average PR and the classical diffusion coefficient. However, more detailed investigations are needed to make any positive statements. The sharp deviation for $R=2$ can be accounted for as due to the presence of an extra quantum symmetry discussed above.

Following our study of the average PR and its scaling with the classical diffusion coefficient, we may then enquire about how the PR itself is distributed in a given spectrum if the average reflects the general behavior. We find that when the classical system is chaotic the distribution of the normalized quantity $y=\ln\xi_2^{-1}/\langle\ln\xi_2^{-1}\rangle$ (this is similar to the distribution of the entropy due to the linear relationship exhibited above) is nearly normal, as seen in Fig. 7. This may be attributed to a realization of the central limit theorem. However the PRs and inverse participation ratios (IPRs) themselves are not normal. Their distributions may be obtained by assuming that the distribution of y is normal. Thus the PRs are distributed according to the log-normal distribution [23]

$$\Lambda(\xi_2^{-1}) = \frac{1}{\sqrt{2\pi}\sigma\langle\ln\xi_2^{-1}\rangle\xi_2^{-1}} \exp\left\{-\frac{1}{2\sigma^2}\left(\frac{\ln\xi_2^{-1}}{\langle\ln\xi_2^{-1}\rangle}-1\right)^2\right\} \tag{26}$$

where σ^2 is the variance of y. As an immediate consequence, the distribution of the IPRs is also log-normal. The distribution of such localization measures is of great significance. Recently, the distribution of IPRs has been exploited to show that the distribution of resonance widths in wave-chaotic dielectric cavities is log-normal [24].

When K is small ($\leqslant 1$), the classical motion is nearly regular for $R=1$, and chaotic for $R\leqslant 0.5$. However, the time scale for classical diffusion is large, making the observation of R effects on quantum dynamics difficult. For instance, the nearest neighbor spacing distribution may remain very close to the Poisson distribution. In such a situation we find that the distribution of the PRs provides a positive litmus test. In

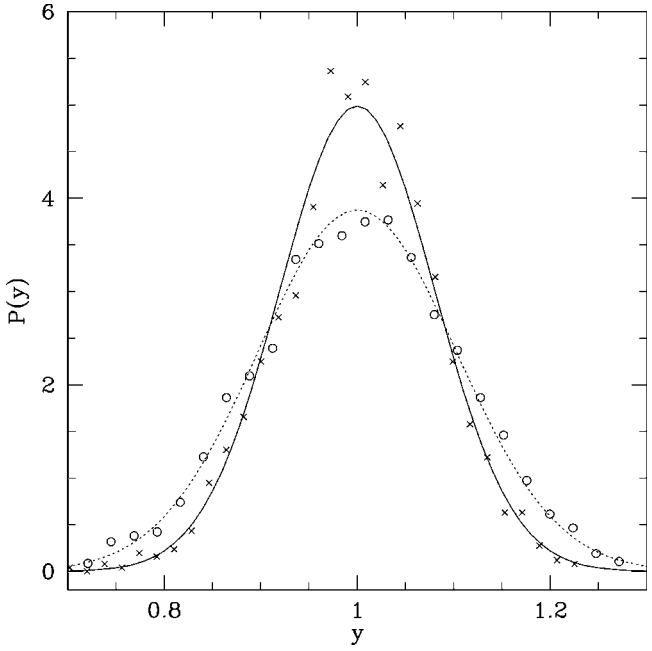

FIG. 7. Probability distribution of y, the normalized logarithm of the PR, for the kicked rotor case ($R=1$) in the chaotic regime. Here we have taken $K=10$ and $\tau=0.025$ ($\times$), $\tau=0.05$ ($\bigcirc$). Smooth curves are corresponding Gaussian distributions.

Fig. 8 such an example is shown, where even for small field strengths the effect of R is clearly visible as a tendency for y to be normally distributed. This is an indication of the ''delocalization'' that is taking place in the eigenfunctions. This delocalization is limited in the sense that while the eigenfunctions remain square integrable there is more spreading out in the bulk part of the states. Thus we may conclude that the distribution of the localization measures is a sensitive quantity in chaotic quantum systems.

The time evolution of nonstationary states must reflect the properties of the stationary states and is also of importance in the context of experiments. Here we have studied the diffusion in kinetic energy of a state $|\Psi\rangle$ that is initially the ground state of the unperturbed system. We illustrate with one example wherein for a fixed classical parameter K the effects of noninteger R are seen clearly for a given τ value. Thus tuning R essentially tunes λ since a is fixed through the relation (11). In Fig. 9 the scaled kinetic energy $\langle P^2\rangle = \langle\Psi|P^2|\Psi\rangle$ is shown as a function of time (number of kicks) for a small value of K corresponding to a small classical field strength ϵ. We note that while the quantum diffusion saturates at a much higher value for $R=1.5$, compared to $R=1$, the actual classical field strength ϵ [from Eq. (4)] is *smaller* by a factor of 1.5. For comparison we show another integer case, $R=2$, where the classical diffusion is smaller than for $R=1$.

B. Eigenvalues and eigenstates

It is clear from our earlier observations that the states are more localized in the regular or mixed regimes of the classical system and less localized (or delocalized) in the chaotic regimes. The degree of localization is also controlled by the ratio of the length scales and the complexity of the classical phase space is reflected in the localization measures. Here we look at the quasienergies and the corresponding states more closely.

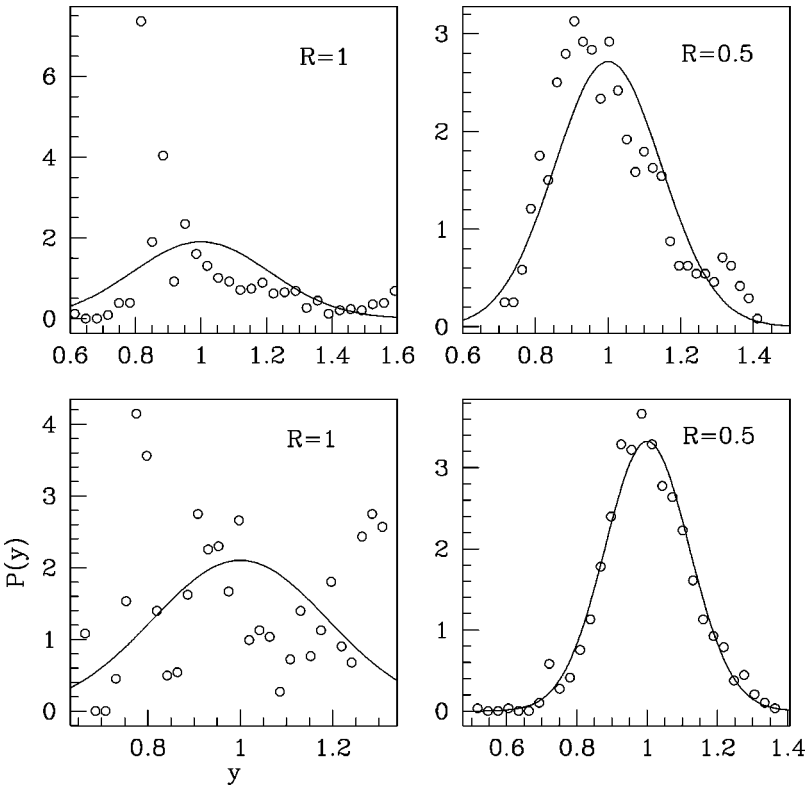

FIG. 8. Probability distribution of y, the normalized logarithm of the PR, for the case $K=0.1$, $\tau=0.001$ (first row) and for $K=1$, $\tau=0.01$ (second row). Smooth curves are corresponding Gaussian distributions. Note the sensitivity of these distributions to the classical dynamics.

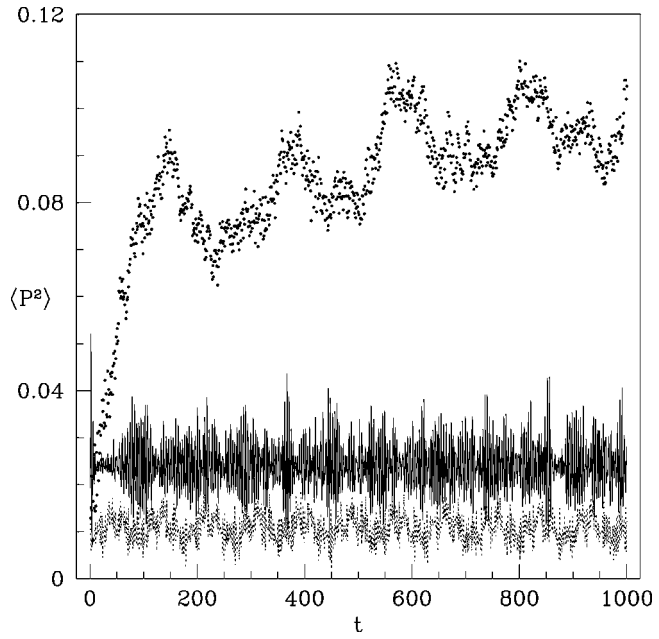

FIG. 9. Shown is the scaled kinetic energy $\langle P^2 \rangle$ of a state that is initially the ground state of the unperturbed system, as a function of time. Here the parameters are $K=1$, $\tau=0.01$; $R=1$ (solid line), $R=1.5$ (dots), and $R=2$ (dotted line). The effect of noninteger R is clearly seen in the evolution as the kinetic energy of the quantum particle saturates at a much higher value compared to the integer R cases.

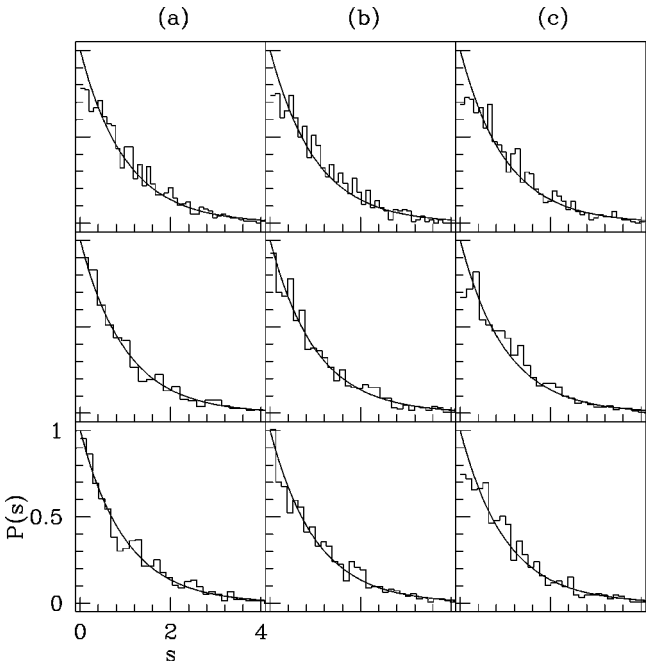

FIG. 10. Nearest neighbor spacing distributions of 1000 quasienergies for (a) $K=0.1$, $\tau=0.001$, (b) $K=1$, $\tau=0.01$, (c) $K=10$, $\tau=0.1$, with $R=0.5,1,1.5$ (top to bottom) and $N=1200$. Smooth curves are Poisson distributions. Note the relative insensitivity of these distributions to the classical dynamics.

In Fig. 10 we show the nearest neighbor spacing distribution of the quasienergies for various parameters. The first row and the last column of the figure correspond to classically chaotic regimes and the rest belong to regular/mixed phase space regimes. In regular/mixed regimes where the states are highly localized, the spacing shows excellent agreement with the Poisson distribution. On the other hand, in chaotic regimes the spacing agrees well with the Poisson distribution except at small spacings. This is due to the fact that the bulk part of the eigenstates is delocalized and they overlap each other. However, the tail parts of the states are exponentially localized and the degree of overlap is not significant enough. We also notice that the spacing distribution is only slightly sensitive to the nature of the classical dynamics in the case of the unbounded kicked rotor or the well, at least in the parameter regimes we have investigated. In such situations, as we have demonstrated earlier, the distribution of PRs is a good measure to distinguish chaotic quantum systems from regular systems.

Our extensive calculations of the eigenstates in chaotic regimes show that, in general, it is hard to qualitatively differentiate the states corresponding to noninteger R values from the rotor ($R=1$) states as far as their localization behavior is concerned. In particular, it is not easy to distinguish the emergence of nonexponential tails unequivocally. However, we found that eigenstates corresponding to noninteger R values generally have more fluctuations compared to the rotor states; this is illustrated with some examples in Fig. 11. The fluctuations are closer to the random matrix theory (RMT) predictions in the case of noninteger R values; this is discussed further below.

Recently there have been studies of the special case ($R=0.5$) of the system (2), with the motivation of revealing quantal behavior of non-KAM systems [17]. It was observed that the quasienergy states are ''extended'' in the unperturbed basis and as a result the spacing was shown to be Wigner distributed. At this juncture we would like to compare our results with certain aspects of this work. In [17], the eigenstate shown in the highly chaotic regime ($K=50$, $N=1024$; we have not been able to ascertain the value of τ used in this work) does *not* appear to belong to the unbounded phase space as it spreads all over the basis. Thus, while states such as these may belong to some truncated dynamical system, they do not belong to the infinite Hilbert space of the well system. Increasing the dimensionality of the matrix used will modify such states; in short, they are not converged. As we demonstrate below, unconverged or poorly converged states may mislead us in understanding the spectrum.

Large K implies large k for given R and τ, and hence our calculation demands bigger dimensionality N of the truncated Hilbert space, since the PR is roughly increasing as k^2. Although we take $N=2000$, getting a good number of converged states is problematic. We pursue the spacing distribution with a different convergence criterion for the states obtained numerically. The convergence criterion uses the partial sum of the state components:

$$\{\mathrm{Sum}\}_M = \sum_{n=1}^{M} |\psi_n|^2 \quad \text{with} \quad M < N. \tag{27}$$

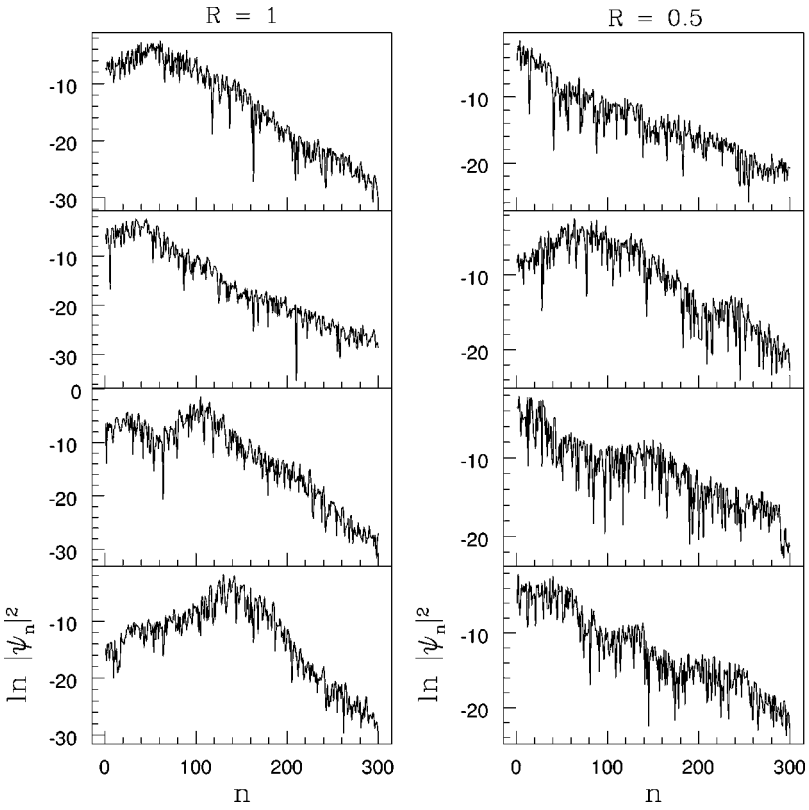

FIG. 11. Typical eigenstates for the case $K=10$, $\tau=0.1$. States corresponding to $R=0.5$ have more fluctuations compared to the rotor ($R=1$) states.

For a well converged state we expect that $\{\mathrm{Sum}\}_M \approx 1$, even for $M \ll N$. We denote by N_M the number of converged eigenstates whose $\{\mathrm{Sum}\}_M$ is greater than S_M (an arbitrary number close to, but less than, unity) for a fixed value of M. Thus the convergence criterion is characterized by M and S_M.

In Fig. 12, we show the spacing distributions with different criteria for two cases. In both cases the transition to the

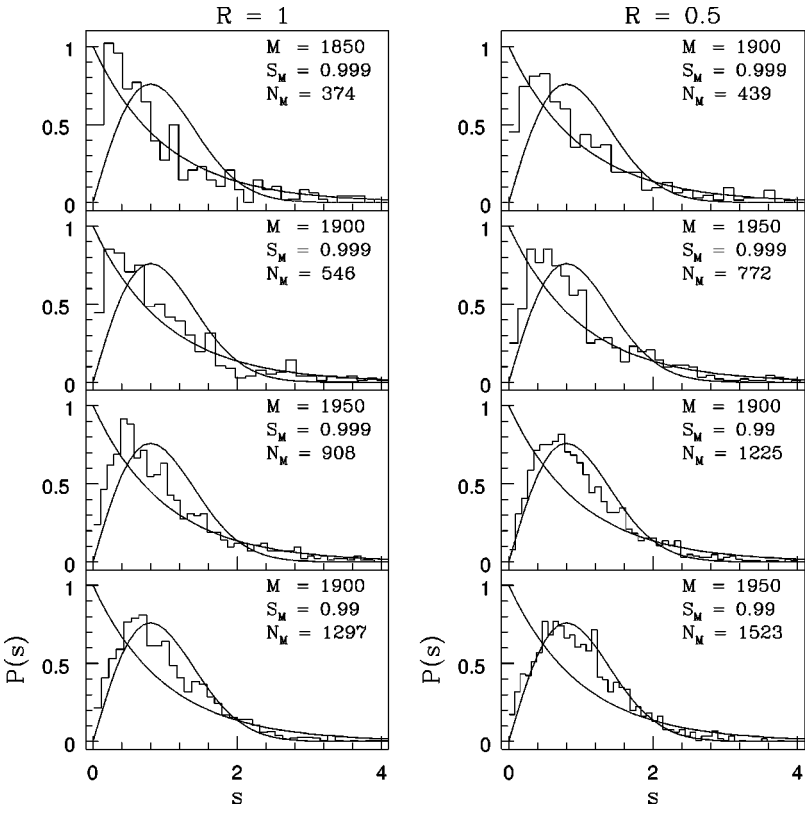

FIG. 12. The nearest neighbor spacing distributions for the case $K=50$, $\tau=0.1$. Smooth curves are the Poisson and Wigner distributions. The convergence criterion is relaxed as we move from top to bottom. A ''spectral transition'' is observed.

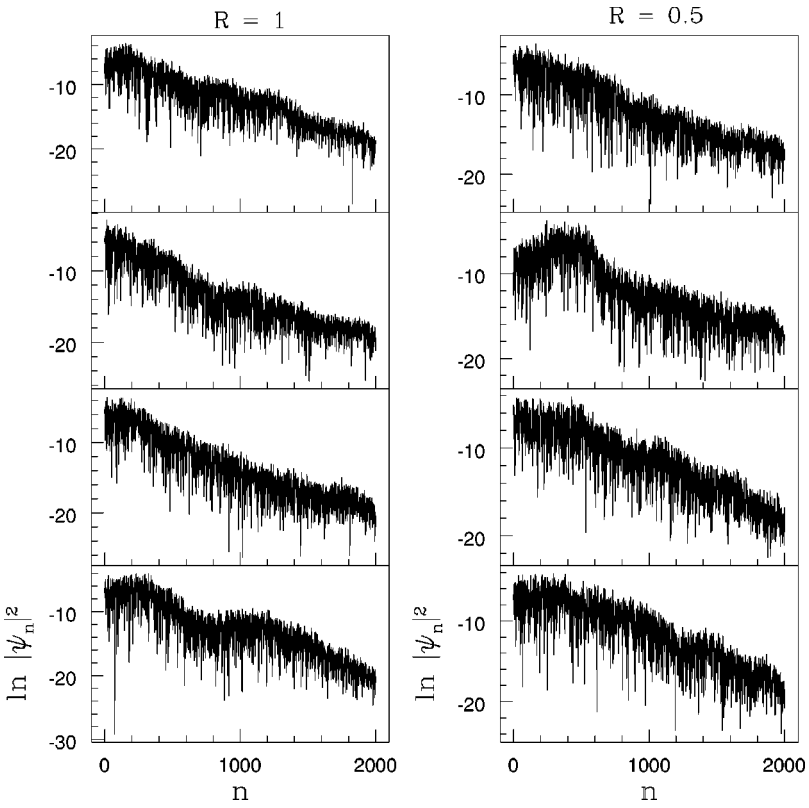

FIG. 13. Typical well converged eigenstates for the highly chaotic case: $K=50$, $\tau=0.1$, and $N=2000$.

Wigner distribution is evident as the convergence criteria is relaxed. The unconverged or poorly converged states do not belong to the physical system of our interest and the corresponding quasienergies follow the RMT prediction. Obviously, the result is more reliable in the top plots where the spacing shows neither a Poisson nor a Wigner distribution. Although the tail part shows Poisson behavior there are significant discrepancies in the small spacing. A more correct picture may be closer to the scenario of the chaotic regimes presented in Fig. 10.

Shown in Fig. 13 are a few ''well converged'' states, with a more stringent convergence criterion ($M=1600$, $S_M=0.9999$). With this criterion we have only $N_M=12$ and 4 for $R=1$ and 0.5, respectively. The state components exhibit strong fluctuations in the basis. Here again it is hard to differentiate the two cases qualitatively. The states corresponding to $R=0.5$ also appear to have exponential tails. To see the distribution of the state components, we introduce a variable $\eta_n=|\psi_n|^2/\overline{|\psi_n|^2}$ where the overbar stands for the average over the state components such that $\overline{\eta}=1$. As seen from Fig. 14, the cumulative distribution of η for both cases is very similar. Considerable deviations from the RMT predicted cumulative Porter-Thomas distribution $I(\eta)=\mathrm{erf}(\sqrt{\eta/2})$, may be attributed to the localization of the states. However, the distribution corresponding to $R=0.5$ tends to be closer to the RMT predicted behavior.

V. SUMMARY AND CONCLUSION

A particle inside a one-dimensional infinite square well potential in the presence of a time-periodic pulsed field is examined both classically and quantum mechanically. This simple model can be seen as one generalization of the kicked rotor, or the standard map. A variety of classical dynamical features emerge from the nature of the ratio R of the two competing length scales (the well width and field wavelength). Many of the dynamical features so observed are ge-

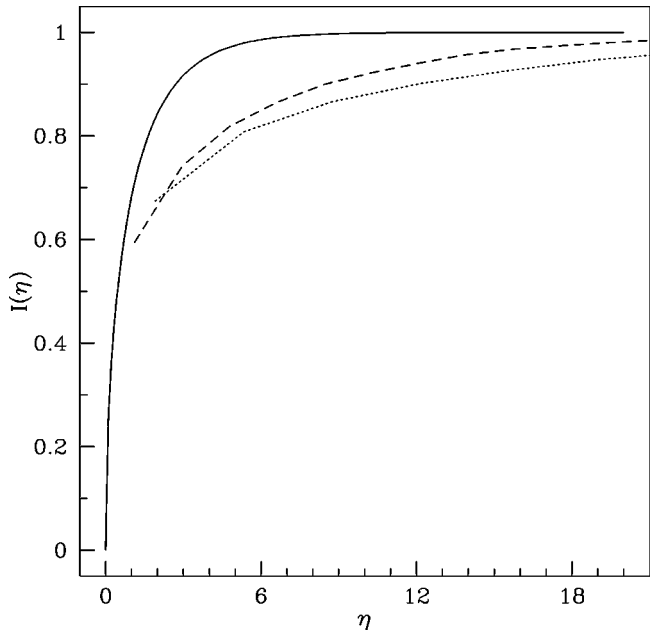

FIG. 14. Collective cumulative distribution of the components of the states shown in Fig. 13. Dotted curve corresponds to $R=1$ while dashed curve corresponds to $R=0.5$. Solid curve is the cumulative Porter-Thomas distribution.

neric to a wide class of systems of substantial current interest, viz., externally forced particles in wells.

It is shown that when the length scales do not match, even in perturbative regimes the dynamics can be increasingly complex wherein all the KAM tori in phase space break up. As a result the transition to chaos is abrupt, a typical scenario of non-KAM behavior. Quantum mechanically, the imprint of such a transition is seen as a spread in the bulk part (delocalization) of the eigenstates. Thus we realize the length scale ratio R as a control parameter for localization in the weak field regime.

On increasing the field strength, chaos assisted diffusion takes place in momentum. From earlier studies of the kicked rotor it is known that the average localization length of the eigenstates is directly proportional to the classical diffusion coefficient. We have shown that in our generalization of the kicked rotor also this result grossly explains the localization behavior of the eigenstates through the classical transport properties. Thus the kicked rotor continues to serve as a useful model in understanding physical phenomena exhibited by a larger class of systems.

We have observed, as expected, that in the regular case the nearest neighbor spacing distribution of the quasienergies show good agreement with the Poisson distribution. We have presented evidence to support the suggestion that, in highly chaotic regimes, the spacings show some deviations from the Poisson distribution although the corresponding eigenstates belong to an unbounded phase space. Limited overlap of the eigenstates results in such deviations. However, the spacing does not show the RMT predicted Wigner distribution as was claimed in an earlier study [17]. The earlier result is attributed to lack of converged states in the statistics.

While the spacing is not very sensitive to classical chaos, the distribution of participation ratios of the eigenstates is shown to be a good measure to distinguish chaotic quantum systems from regular ones. Quantum mechanically, chaotic regimes are characterized by a log-normal distribution of the participation ratios. In addition to the above generic quantum features, we have also studied nongeneric phenomena like ''quantum resonance.'' In the resonance condition, the kinetic energy of the particle grows quadratically with increasing number of kicks. This unbounded energy growth is not affected by the length scale ratio and can enhance ionization in the finite well system.

As far as experimental realization of this work is concerned, perhaps both quantum wells [3] and cold atom experiments [15] are possible candidates. As suggested above, the R effects may be best observed at small field strengths and for $R>1$. Further work is underway exploring the nature of localization in such systems, including a bounded version of the generalized standard map.

[1] F. Haake, *Quantum Signatures of Chaos* (Springer-Verlag, Berlin, 1991).

[2] H-J. Stockmann, *Quantum Chaos: An Introduction* (Cambridge University Press, Cambridge, 1999).

[3] P. B. Wilkinson, T. M. Fromhold, L. Eaves, F. W. Sheard, N. Miura, and T. Takamasu, Nature (London) **380**, 608 (1996).

[4] L. E. Reichl, *The Transition to Chaos* (Springer, New York, 1992).

[5] M. V. Berry, N. L. Balazs, M. Tabor, and A. Voros, Ann. Phys. (N.Y.) **122**, 26 (1979).

[6] G. Casati, B. V. Chirikov, F. M. Izrailev, and J. Ford, in *Stochastic Behavior in Classical and Hamiltonian Systems*, Lecture Notes in Physics Vol. 93 (Springer-Verlag, Berlin, 1979), p. 334.

[7] B. V. Chirikov, Phys. Rep. **52**, 263 (1979); Rev. Plasma Phys. **13**, 1 (1987).

[8] J. M. Greene, J. Math. Phys. **20**, 1183 (1979).

[9] S. J. Shenker and L. P. Kadanoff, J. Stat. Phys. **27**, 795 (1982).

[10] A. J. Lichtenberg and M. A. Lieberman, *Regular and Chaotic Dynamics* (Springer, New York, 1992).

[11] F. M. Izrailev, Phys. Rep. **196**, 299 (1990).

[12] A. Lakshminarayan, N. R. Cerruti, and S. Tomsovic, Phys. Rev. E **60**, 3992 (1999); **63**, 016209 (2001).

[13] D. R. Grempel, R. E. Prange, and Shmuel Fishman, Phys. Rev. A **29**, 1639 (1984).

[14] P. W. Anderson, Phys. Rev. **109**, 1492 (1958).

[15] F. L. Moore, J. C. Robinson, C. F. Bharucha, Bala Sundaram, and M. G. Raizen, Phys. Rev. Lett. **75**, 4598 (1995); J. Ringot, P. Szriftgiser, J. C. Garreau, and D. Delande, *ibid.* **85**, 2741 (2000).

[16] T. A. Brody, J. Flores, J. B. French, P. A. Mello, A. Pandey, and S. S. M. Wong, Rev. Mod. Phys. **53**, 385 (1981).

[17] Bambi Hu, Baowen Li, Jie Liu, and Yan Gu, Phys. Rev. Lett. **82**, 4224 (1999).

[18] R. Sankaranarayanan, A. Lakshminarayan, and V. B. Sheorey, Phys. Lett. A **279**, 313 (2001).

[19] Ya. B. Zel'dovich, Sov. Phys. JETP **24**, 1006 (1967).

[20] F. M. Izrailev and D. L. Shepelyanskii, Theor. Math. Phys. **43**, 553 (1980).

[21] B. V. Chirikov, F. M. Izrailev, and D. L. Shepelyansky, Sov. Sci. Rev. **2C**, 209 (1981).

[22] D. L. Shepelyansky, Phys. Rev. Lett. **56**, 677 (1986); Physica D **28**, 103 (1987).

[23] J. Aitchison and J. A. C. Brown, *Lognormal Distribution: With Special Reference to its Uses in Economics* (Cambridge University Press, Cambridge, 1957).

[24] O. A. Starykh, P. R. J. Jacquod, E. Narimanov, and A. D. Stone, Phys. Rev. E **62**, 2078 (2000).